RSC Advances

PAPER

View Article Online
View Journal | View Issue

Cite this: *RSC Adv.*, 2024, **14**, 2621

Further study on particle size, stability, and complexation of silver nanoparticles under the composite effect of bovine serum protein and humic acid

Yu-jing Qiao,[a] Jia Kang,*[b] Chu-qiong Song,[c] Ning Zhou,[b] Peng Zhang[b] and Gang-fu Song[b]

Silver nanoparticles (AgNPs) are widely used due to their unique antibacterial properties and excellent photoelectric properties. Wastewater treatment plants form a pool of AgNPs due to the social cycle of wastewater. During biological treatment processes, the particle size and stability of AgNPs change. We studied the particle size changes and stability of silver nanoparticles in the presence of bovine serum albumin (BSA) and humic acid (HA). The experimental results indicated that silver nanoparticles can complex with the functional groups in BSA. For AgNP–BSA composites, as the BSA concentration increases, the size of the silver nanoparticles first decreases and then increases. AgNPs can combine with the amide, amino, and carboxyl groups in HA. As the concentration of HA increases, the particle size and large particle size distribution of AgNPs increase. This increasing trend is more obvious when the HA concentration is lower than 20 mg L^{-1}. When HA and BSA exist at the same time, HA will occupy the adsorption sites of BSA on the surface of AgNPs, and the AgNP–HA complex will dominate the system. This study aims to provide key operational control strategies for the process operation of wastewater treatment plants containing AgNPs and theoretical support for promoting water environment improvement and economic development such as tourism.

Received 10th September 2023
Accepted 20th December 2023

DOI: 10.1039/d3ra06159k

rsc.li/rsc-advances

1. Introduction

Nanosilver's unique antibacterial properties and excellent photoelectric properties make it widely used in textile manufacturing, food production, medical industry, and other fields.[1] This also leads to the enrichment of nanosilver in the atmosphere, soil, and water.[1,2] Water bodies are the final destination for nanosilver.[3] Silver nanoparticles (AgNPs) enter water bodies through sewage discharge, atmospheric dry and wet deposition, and landfill leachate.[4] AgNPs that enter the water environment usually do not exist permanently. They collide with each other and aggregate under the action of the Brownian motion of the water column, fluid motion, and differential sedimentation.[5] Common surfactants, such as PVP and citrate, can form a coating on the surface of AgNPs, which will increase the surface charge of AgNPs and enhance the stability of nanosilver colloids in water.[6] Dissolved organic matter is also an important factor affecting the stability of AgNPs in water.[7] The proportion of functional groups in dissolved organic matter, such as non-polar aliphatic carbon, aromatic carbon, and phenolic carbon, and the molecular weight of dissolved organic matter affect the aggregation of AgNPs by affecting the size of the nanoparticles.[8]

The suspended solids in wastewater can provide a large attachment area for AgNPs, and hence, the AgNPs entering the wastewater are adsorbed onto the suspended solids or precipitate on the suspended solids in the form of colloids.[9,10] The presence of a large amount of organic matter in sewage leads to more obvious changes in AgNPs in sewage. Soluble microbial products (SMPs) (mainly composed of humic acid (HA) and protein) in sludge can capture AgNPs. Due to the complexation of SMP and AgNPs, a large number of AgNPs accumulates on the surface of the sludge floc.[11] Dasgupta *et al.*[12] have shown that one or two protein molecules will bind to the sides or ends of AgNPs. This process is related to the hydrophobic amino acids in the protein. The larger the size of AgNPs, the larger the binding constant of bovine serum albumin (BSA)–AgNPs.[13] Qiu *et al.* found that the presence of HA can also enhance the aggregation of AgNPs, which reduces the toxicity of AgNPs to microorganisms in activated sludge.[14] However, HA increases the sulfidation rate of AgNPs by increasing the surface area available for vulcanization on the surface of AgNPs, which also

[a]*Physical Education College of Zhengzhou University, Zhengzhou 450044, China*
[b]*School of Environmental and Municipal Engineering and Ural Institute, North China University of Water Resources and Electric Power, Zhengzhou 450046, China. E-mail: kangjia@ncwu.edu.cn*
[c]*Henan Urban Planning and Design Institute Co., Ltd, Zhengzhou 450044, China*

reduces the toxicity of AgNPs to microorganisms in activated sludge.[15]

Most of the existing research focuses on the impact of the presence of AgNPs on the sewage treatment process, but there is less research on the changes that occur during the sewage treatment process. This study uses BSA and HA as simulants of dissolved organic matter in sewage treatment plants and uses the concentration levels in sewage treatment as a reference to explore the changes in particle size and stability of AgNPs under the individual and combined effects of the two situations, summarize the complexation mechanism, and provide theoretical support and key operation control strategies for the process operation of sewage treatment plants containing nanosilver.

2. Materials and methods

2.1 Preparation of silver nanoparticles

Silver nitrate ($AgNO_3$, CAS: 7761-88-8), trisodium citrate ($C_6H_5Na_3O_7$, CAS: 6132-04-3), sodium borohydride ($NaBH_4$, CAS: 16940-66-2), sodium phosphate monobasic (NaH_2PO_4, ≥99%) and sodium phosphate dibasic (Na_2HPO_4, ≥99.0%) were obtained from Tianjin Kemiou Chemical Reagent Co., Ltd (Tianjin, China). Bovine serum albumin (BSA, 96%, CAS: 9048-46-8) and humic acid (HA, ≥90%, CAS: 1415-93-6) were procured from Shanghai McLean Biochemical Technology Co., Ltd (Shanghai, China).

A certain amount of BSA was dissolved in 0.01 M phosphate buffer solution (PB, pH 7.4), from which the BSA stock solution of 2 g L^{-1} was prepared. There was 1.0 g of HA added to the 10 mM NaOH solution after continuous stirring on the magnetic stirring apparatus for 30 min at a constant volume to obtain 1 g L^{-1} of HA stock solution. All the stock solutions were kept in a refrigerator at 0–4 °C.

In the test, citrate-coated AgNPs were synthesized by a chemical reduction method.[16] First, 0.5 mL of $AgNO_3$ (50 mM) and 0.75 mL of $C_6H_5Na_3O_7$ (50 mM) were added to 100 mL of distilled water at 45 °C, respectively. After thoroughly stirring, 10 mL of $NaBH_4$ (5 mM) was added dropwise to the mixture and stirred at high speed for 30 min. A bright yellow and brown solution was obtained, which suggested the formation of AgNPs and was stored as the stock solution. The prepared AgNP colloid from the water bath heating pot was ultrasonically oscillated for 20 min to prevent oxidation and aggregation.

2.2 Instruments and characterization

Transmission electron microscopy (TEM) was performed using a JEOL-2010 (LaB6 filament) electron microscope at an accelerating voltage of 120 kV. Absorption spectral analysis was performed using a UV-2501PC Shimadzu spectrophotometer with 1 cm path length quartz cuvettes and a scanning range of 200–800 nm. The hydrodynamic diameter and zeta potential of AgNPs were measured using a Malvern Zetasizer Nano S90 and a ZETA-check instrument, respectively. The Fourier transform infrared (FTIR) spectra were recorded using a Bruker TENSOR 37 in the 500–4000 cm^{-1} range. Three-dimensional fluorescence spectra were measured and analyzed using an RF-6000 machine.

2.2.1 Transmission electron microscope (TEM) imaging. TEM samples were prepared by dropping a AgNP sol (3.774 mg L^{-1}) onto carbon-coated copper grids. The suspended material on the TEM grid was allowed to dry before measurement. The TEM images can explain the shape and dispersion degree of AgNPs prepared in the solution.[17]

2.2.2 UV-vis spectrum wavelength scanning. The plasmonic resonance effect of the electron cloud on the surface of AgNPs leads to its unique characteristic absorption peak in UV-vis wavelength scanning, and the peak type and absorption intensity of the absorption peak are closely related to the particle size, shape, and dispersion of AgNPs in the system. Therefore, UV-vis spectroscopy is commonly used to determine whether AgNPs exist in the system and to speculate on the shape and structure characteristics of AgNPs. The variable BSA or HA solution was added to the fixed amount of AgNP sol (3.774 mg L^{-1}), and the content of BSA in the system was 0, 50, 100, 150, 300, 600, and 1000 mg L^{-1}, and the HA content was 0, 10, 20, 50, 100, and 150 mg L^{-1}. The influence of BSA and HA on the existence state of AgNPs was determined by studying the change in the plasma resonance peak of AgNPs before and after the addition of BSA and HA. Deionized water was used as a blank control in all experiments.

2.2.3 Hydrodynamic diameter and zeta potential measurements. For the charged amount of AgNPs at different pH values (1–10), a value was measured every 30 s using a zeta potentiometer, and the same sample was measured three times and the average value was taken. At the same time, the zeta potentials of the AgNPs were measured at different concentrations of BSA and HA. Before the measurement, the pH values of AgNP–BSA and AgNP–HA mixtures were adjusted to 4, 6, 9, and 2, 4, and 6, respectively, to study the charged amounts of the mixtures under different pH conditions.

The size distribution of nanomaterials in the solution can be determined using dynamic light scattering (DLS), which provides the hydrodynamic diameter of nanoparticles and the size distribution based on numbers. For each sample, five measurements were performed using DLS at a laser wavelength of 633 nm with an acquisition time of 20 seconds to obtain the average hydraulic particle size and particle size distribution of the AgNPs.

2.2.4 Fourier transform infrared (FTIR) spectroscopy. FTIR spectroscopy of proteins helps study the changes in protein secondary structure based on spectral shifts and changes in protein amide bands.[18] Fourier transform infrared spectroscopy was performed to analyze the composition and content of the main functional groups before and after adding BSA or HA. The samples were freeze-dried for 48 hours in advance and then fully ground with KBr in a ratio of 1 : 100.

2.2.5 Three-dimensional fluorescence spectroscopy (3D-EEM). In this work, 3D-EEM is the most commonly used technique to study the conformational changes of proteins. It can display the fluorescence information of samples more comprehensively and analyze the conformational changes and the composition of samples. It is a highly sensitive and selective

measurement method. The excitation wavelength (λ_{Ex}) of the 3D-EEM was set at 200–500 nm, the emission wavelength (λ_{Em}) was set at 200–550 nm, the scanning speed was 600 nm min^{-1}, and the scanning gap was 5.0 nm.

3. Results and discussion

3.1 Characterization and analysis of AgNPs

The UV-vis wavelength scanning diagram is shown in Fig. 1(a), in which it can be clearly seen that a strong absorption band is formed at λ_{max} = 393 nm, which is consistent with the absorption peak of the resonance of AgNPs at λ_{max} = 390–420 nm obtained in the literature. Meanwhile, the research shows that the smaller the particle size of AgNPs, the more the position of the outgoing peak of the absorption peak moves in the direction of the decreasing wavelength, indicating that AgNPs with a smaller particle size are prepared by the system.[19] As can be seen from the figure, the absorption peak of AgNPs prepared in this study is sharp and symmetrical, and the half-peak width is small. According to the small half-peak width of the maximum absorption peak and the symmetrical and strong peak shape, the size distribution range of the prepared AgNPs is more concentrated, and the uniformity is better. The results indicated that the prepared AgNPs belonged to monodisperse spherical AgNPs with a narrow and focused size distribution range.[20] By recording the TEM images of AgNPs coated with citric acid (Fig. 1(b)), it can be found that the prepared AgNPs are nearly spherical or elliptical, with a size between 5 and 25 nm, and have good dispersion stability among nanoparticles. This is consistent with the form and dispersion of AgNPs described by Pillai.[21]

DLS is the most common analytical method used for nanoparticle size estimation. The DLS analysis of synthesized AgNPs is shown in Fig. 1(c). The hydrodynamic diameter of AgNPs is 20.5 nm, and the obtained value is well supported by the value already reported in the literature.[22]

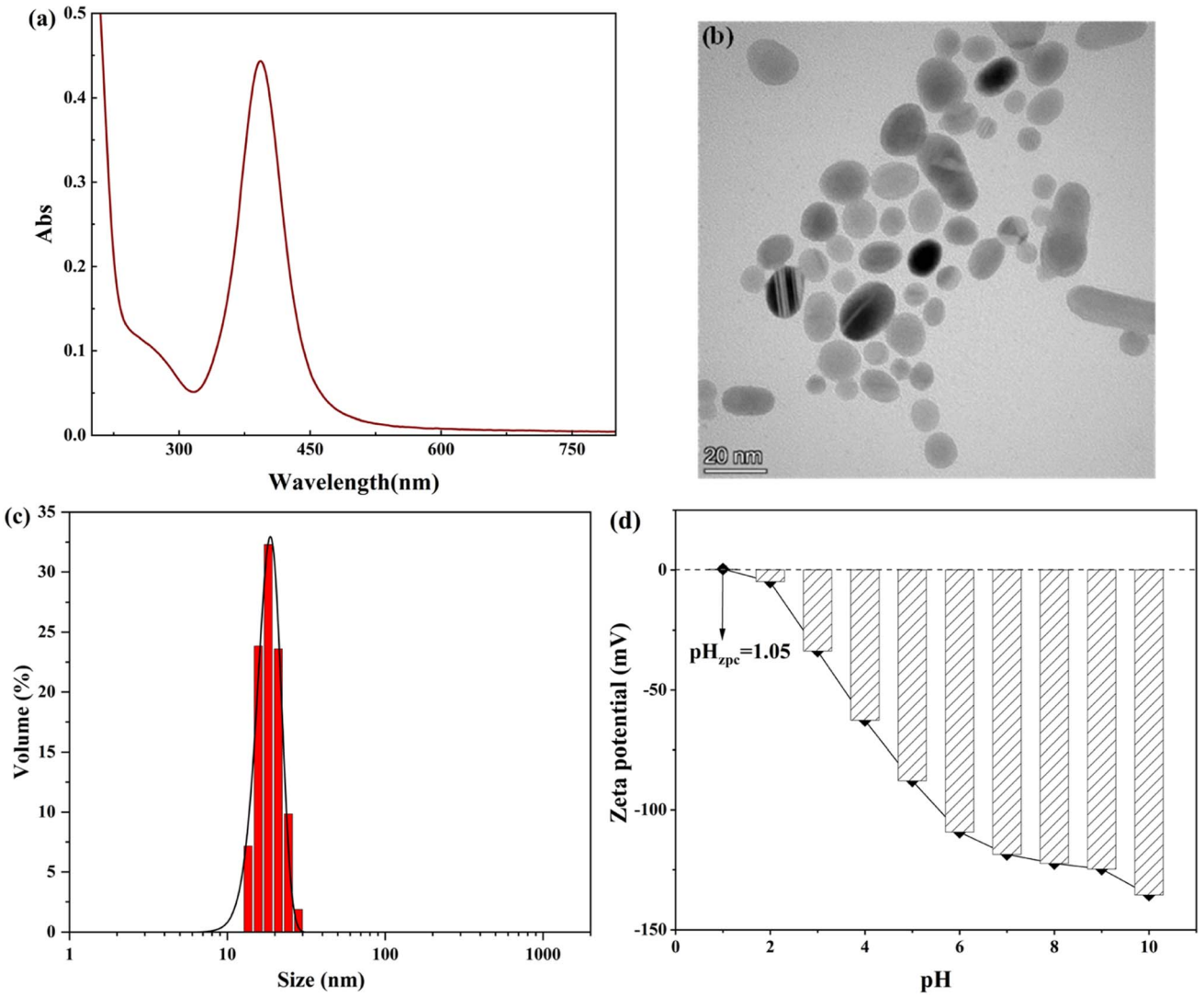

Fig. 1 (a) UV-vis absorption spectra of AgNPs. (b) TEM images of AgNPs. (c) Size distribution map of AgNPs. (d) Zeta potential of AgNPs as a function of pH.

It can determine the stability and zero-point potential of nanoparticles with the help of the zeta potential, and the measured charge on the surface of nanoparticles judges the magnitude of interparticle repulsion. The variation in zeta potential of AgNPs sols at different pH values was determined experimentally. As shown in Fig. 1(d), when pH = 3.0, the AgNPs had a $|\zeta| > 30$ mV, indicating that the AgNPs at this time had good stability performance in the system and a large number of negative charges were gathered on the surface of the nanoparticles.[23] With the increase in the pH of the solution, the zeta potential value of AgNPs keeps decreasing, and AgNPs are becoming increasingly stable in the system. When pH = 1.0–2.0, the surface charge of AgNPs changes from positive to negative, and the isoelectric point of AgNPs is presumed to be pH = 1.05; at this pH, the surface positive and negative charges of AgNPs are precisely equal, the morphology of AgNPs is the most unstable, and the solubility is the smallest, the particles are elementary to combine into larger aggregates because of van der Waals. This conclusion is also consistent with the findings of He *et al.*[24] The positive charge on the surface of AgNPs when pH < 1.0 mainly due to the increasing concentration of H^+ in the solution under a strongly acidic environment makes the AgNPs adsorb a large amount of H^+ on the surface. The negative surface charge is neutralized, which leads to a decrease in the absolute value of the potential on the AgNP surface, and AgNPs agglomerate in the solution.[25]

The characterization and analysis studies of the prepared AgNPs using UV-vis spectroscopy, TEM analysis, DLS, and the zeta potential method showed that the chemical reduction method with $NaBH_4$ as the reducing agent and $C_6H_5Na_3O_7$ as the protecting agent could prepare AgNPs with a spherical structure and a particle size of 20.5 nm. The AgNPs had good interparticle stability. At the same time, the zeta potential analysis of AgNPs showed that the environment more obviously changes the existence state of the prepared AgNPs. The interparticle became extremely unstable and easily agglomerated in a strongly acidic environment. Still, with the increase in the pH of the solution, AgNPs were subsequently stabilized in the solution, indicating that the prepared AgNPs were more suitable for maintaining good particle stability in weakly acidic and alkaline environments.

3.2 Characterization and analysis of AgNP interaction with BSA

Fig. 2(a) shows the evolution of the binding to the AgNPs in the presence of BSA by variation in the spectral band and the absorption intensity using UV-vis absorption spectra. As can be seen in Fig. 2(a), the addition of BSA molecules led to the formation of a new absorption band at 280 nm, which is the absorption peak caused by the aromatic amino acid residues (tryptophan and tyrosine) in BSA.[26] With the increase in the concentration of BSA solution, the absorption peaks of AgNPs showed a red shift followed by a blue shift, a phenomenon consistent with the UV results of Mbeta,[27] indicating that the interaction between AgNPs and BSA both occurred and the formed substances existed in solution as AgNPs–BSA complexes;[28] moreover, the absorption intensity of AgNPs with the increase in the BSA concentration showed a trend of increasing and then decreasing, and the color-enhancing effect of the absorption peak could be due to the addition of a low concentration of BSA molecules, which induced Ag^+ to form AgNPs with a smaller particle size.[29] The main reason for the color reduction effect of the plasmon resonance absorption peak of AgNPs may be that the addition of a high concentration of BSA replaces the sodium citrate molecules on the surface of AgNPs to some extent and mosaics them on the surface of AgNPs in the form of inclusions, forming AgNP–BSA complexes and making the AgNP content in solution lower. This substitution of BSA molecules for sodium citrate molecules on the surface of nanoparticles is also known as the substitution hypothesis.[30]

To further determine the structural changes of the AgNPs by adding BSA, we measured the pattern of electrophoretic mobility with pH for different concentrations of BSA added to AgNPs. Fig. 2(b) shows the zeta potential of AgNPs with varying concentrations of BSA under other pH conditions. The zeta potential is positive at lower pH and negative at higher pH. This is because when pH = 4.0, the BSA molecules dissociate into cations in the acidic environment and adsorb onto the surface of AgNPs, making the AgNP surface positively charged. At the same time, with the increase in BSA concentration, the charge on the surface of AgNPs has a complex high and low variation, which is due to the concentration of reactants, indicating that the complex formed by BSA and AgNPs has less electrostatic repulsion and a higher aggregation probability between the particles.[31] By increasing the solution pH, the effect of the change in BSA concentration on the surface charge of AgNPs decreased until the solution pH was increased to 9.0, and it can be seen from the figure that the stability of AgNPs was negatively correlated with the BSA concentration at this time, except for the high concentration of BSA (1000 mg L^{-1}), indicating that in an alkaline environment, the low concentration of BSA is more favorable for the AgNPs in solution stability. Meanwhile, the BSA molecules appeared in the alkaline environment.[26] With the increase in BSA concentration in the system, BSA in the solution aggregated into large molecules that were difficult to attach to the surface of AgNPs as encapsulants, thus leading to decreased AgNP stability.

Meanwhile, the isoelectric point of BSA was found to increase by calculation (from 4.80 to 5.36), indicating that the complexation between the two after adding BSA to AgNPs led to a change in protein conformation and a more spreading structure. However, by changing the solution pH, the isoelectric point of the AgNP–BSA complex formed after the interaction between AgNPs and BSA could be calculated at pH = 5.36 ± 0.2, indicating that near the isoelectric point, the AgNP–BSA complex could be precipitated as a precipitate, laying the foundation for the subsequent study of AgNP and SMP at different pH values.

Fig. 2(c) represents the IR spectra of BSA before and after the interaction with AgNPs, from which it can be seen that the individual BSA molecules are in the 1655 cm^{-1}, 1540 cm^{-1}, 1398 cm^{-1}, 1359 cm^{-1}, 1164 cm^{-1}, and 1072 cm^{-1} bands, which are the amide I band, amide II band, and amide III band,

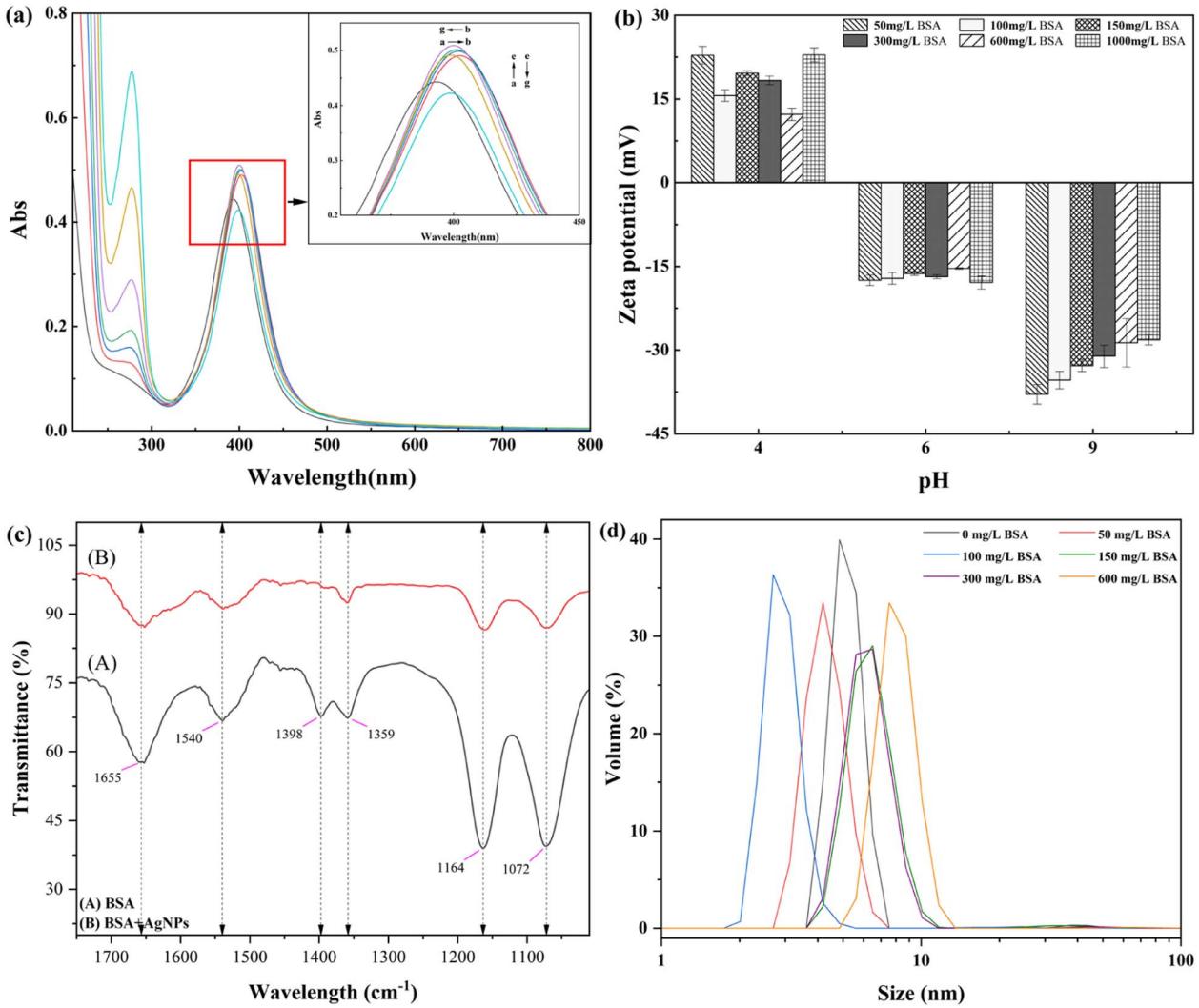

Fig. 2 (a) Surface plasmon resonance absorption of different concentrations of BSA with AgNPs. [AgNPs] = 3.774 mg L^{-1}, a–g: [BSA] = 0, 50, 100, 150, 300, 600, and 1000 mg L^{-1}. (b) Effect of different concentrations of BSA on the zeta potential of AgNPs. (c) Infrared spectra of AgNPs before and after the interaction with BSA. (d) Effect of different concentrations of BSA on the average particle size of AgNPs.

respectively.[32] After adding a certain amount of AgNPs, the characteristic spectra of some functional groups drifted or disappeared, and mainly: (i) the peaks of the protein–peptide bonded amide I band drifted, from which it can be inferred that –C=O and C–N bonds are bonded to AgNPs; (ii) the C–H stretching vibration and N–H bending vibration of the amide II band drifted, which proved that they were also involved in the complexation with AgNPs, but were not the functional groups playing the primary role; (iii) the C–N stretching vibration spectral peak of the amide III band basically disappeared, while the C–N bending vibration spectral peak drifted, which showed that the O and N atoms in the amide were more involved in the complexation with AgNPs. Besides, the spectral peaks dominated by the primary alcohol and carboxyl groups as well as the spectral peaks of the amide band were weakened, indicating that the functional groups that make the main contribution to the complexation reaction of BSA with AgNPs are the amino group, amide group, and carboxyl group, and the complexation of the two directly leads to a reduction in the α-helix content in the secondary structure of the BSA molecule and induces the denaturation of the protein molecule, which causes the conformational change of BSA.[33]

The change in AgNP particle size after the interaction between AgNPs and different concentrations of BSA can be seen in the graph; with the step-by-step increase in BSA concentration, the AgNP particle size showed a trend of decreasing and then increasing (as shown in Fig. 2(d)). When the concentration of BSA rose from 0 to 100 mg L^{-1}, the particle size of AgNPs in the system decreased, and the particle size range increased, especially when BSA = 100 mg L^{-1}. The average particle size of AgNPs decreased from 39.3 nm to 18.9 nm, indicating that the addition of BSA caused the system to produce more small-sized AgNPs, consistent with the above-mentioned UV analysis results. The average particle size of AgNPs in the solution increased to 75.5 nm, as the concentration of BSA increased to 600 mg L^{-1}. Meanwhile, after the reaction of AgNPs with 600 mg L^{-1} of BSA, the DLS

experimental data showed that the particle size distribution of AgNPs in the system was not uniform. This is because BSA undergone a chemical reduction reaction with Ag^{+}, forming small nanoparticles present in the solution. At the same time, high concentration of BSA promoted the aggregation of AgNPs, resulting in the formation of micrometer sized particles present in the solution.

Fig. 3 shows the three-dimensional fluorescence spectra of BSA in the presence of 300 mg L^{-1} BSA and 0, 0.3774, 0.4718, 0.9435, 1.258, 1.887, 4.718, and 9.435 mg L^{-1} AgNPs. The three-dimensional fluorescence data and information before and after the combination of BSA and AgNPs are shown in Table 1. It can be seen from the figure that when there is no presence of the solution AgNPs, BSA shows strong fluorescence intensity at λ_{Em} = 275–445 nm and λ_{Ex} = 205–305 nm. When only 0.3774 mg L^{-1} of AgNPs were added, the fluorescence intensity in BSA showed a substantial decrease, indicating that AgNPs had a burst effect on BSA, and this fluorescence phenomenon indicated that AgNPs interacted with BSA, making the fluorescence intensity of BSA decrease.[33] Based on the changes in the

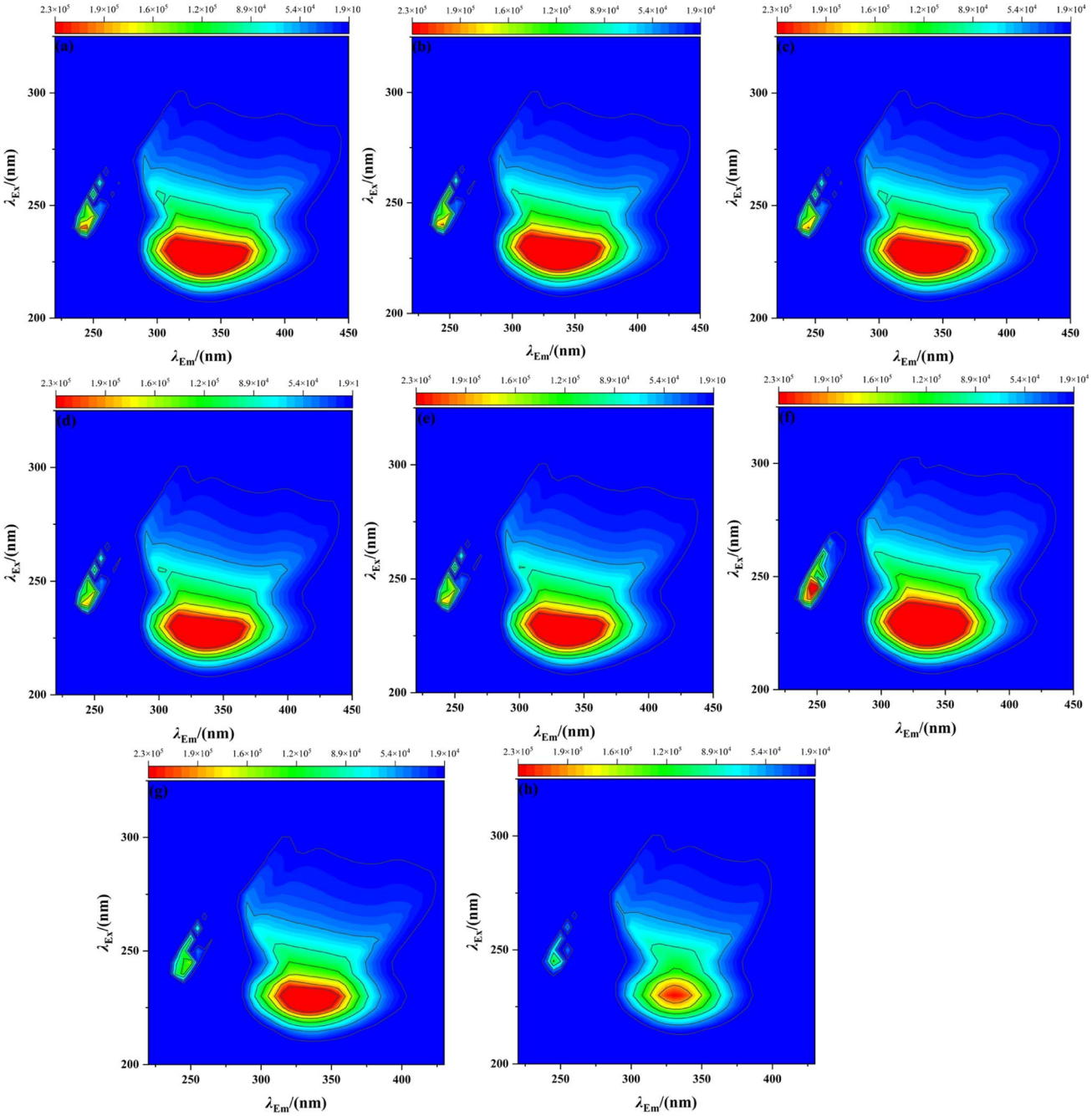

Fig. 3 Three-dimensional fluorescence spectra of AgNPs with BSA at different concentrations. [BSA] = 300 mg L^{-1}, a–h: [AgNPs] = 0, 0.3774, 0.4718, 0.9435, 1.258, 1.887, 4.718, and 9.435 mg L^{-1}.

Table 1 Results of 3D-EEM of bovine serum protein and silver nanoparticles

Concentration of AgNPs (mg L^{-1})	Peak position ($\lambda_{ex}\cdot\lambda_{em}^{-1}$) (nm)	Stokes shift (nm)	Fluorescence intensity ($\times 10^3$)
0	225/335	110	411
0.3774	225/335	110	226
0.4718	225/335	110	313
0.9435	225/335	110	427
1.2580	225/335	110	362
1.8870	230/325	95	367
4.7180	230/325	95	386
9.4350	230/330	100	403

UV absorption spectra of BSA before and after the addition of AgNPs at different concentrations, it indicates that a complex was generated between AgNPs and BSA, which is a static burst, and this result is consistent with the study of Xu *et al.*[34] However, when the concentration of AgNPs was increased to 0.4718 mg L^{-1}, the peak fluorescence intensity of BSA suddenly increased again, indicating that BSA may interact with AgNPs in solution to form a new AgNP–BSA complex. It is expected that this synthesized zeta potentials are consistent with the above-mentioned analysis, indicating that the interaction of BSA with AgNPs leads to protein conformational changes, causing protein denaturation.

3.3 Characterization and analysis of AgNP interaction with HA

From Fig. 4(a), with the addition of HA, the absorption intensity of AgNPs at 393 nm increased from 0.443 to 0.708 (HA = 20 mg L^{-1}), indicating that the bridging interaction (interparticle bridging) between HA and AgNPs led to the production of larger particles;[35,36] meanwhile, with the increase in HA concentration, the absorption peak of AgNPs at 400 nm was gradually asymmetric, and the half-peak width increased, which shows that the addition of HA has affected the existence of AgNPs to some extent. The particles of AgNPs are no longer in

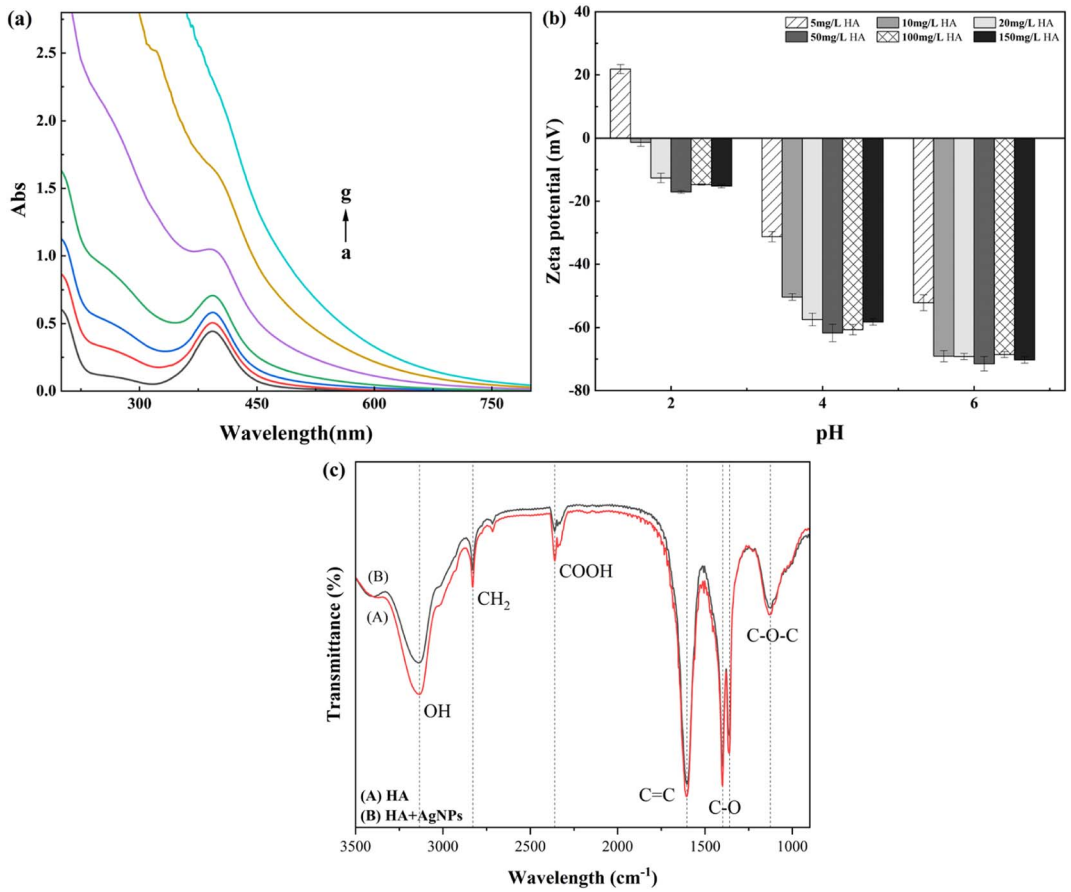

Fig. 4 (a) Surface plasmon resonance absorption of different concentrations of HA with AgNPs. [AgNPs] = 3.774 mg L^{-1}, a–g: [HA] = 0, 5, 10, 20, 50, 100, and 150 mg L^{-1}. (b) Effect of different concentrations of HA on the zeta potential of AgNPs. (c) Infrared spectra of AgNPs before and after the interaction with HA.

the form of monodisperse spheres in the solution. The particle size of AgNPs further increases with the increase in HA concentration, and the particle size distribution of AgNPs increases.[36,37]

It can be seen in the graph of the zeta potential of AgNPs at different concentrations of HA that the presence of HA enhances the electronegativity of AgNPs. The surface potential of AgNPs decreases from the initial −54.8 mV (pH = 6.0) to −70.3 mV since HA is negatively charged[38] and can attach to the surface of AgNPs. At the same time, the AgNP–BSA complex is polymeric, larger than BSA, and may be much smaller than the incident wavelength, so that under the given conditions, the fluorescence intensity was enhanced.[39] When the concentration of AgNPs was increased to 1.887 mg L^{-1}, the excitation wavelength was red-shifted. The emission wavelength was somewhat blue-shifted, indicating that AgNPs are present among the fluorescent groups in the vicinity of BSA. The interaction changes the microenvironment of the fluorescent group near BSA, making the protein molecule more inclined to the folded state and the α-helix content reduced.[39] Meanwhile, the UV spectra of the reaction of different concentrations of AgNPs with BSA and the presumed changes in HA indicates the presence of many phenolic hydroxyl and carboxyl groups and other negatively charged functional groups, and hence, the AgNPs exhibit strong electronegativity. From Fig. 4(b), it can be seen that at the same pH, a low concentration of HA has a more significant effect on AgNPs, probably because a small amount of HA can be adsorbed onto the surface of AgNPs. Still, with the increase in HA concentration, the adsorption on the surface of AgNPs reaches saturation. At this time, the change in HA concentration has little effect on the surface potential of AgNPs, which is consistent with the report of Wu *et al.*[38] At pH = 2.0, after a small amount of HA was added to AgNPs, the surface of AgNPs was positively charged at this time, mainly because HA is insoluble in strong acids. The HA in the solution was easily precipitated in the form of a suspension and neutralized with the charge carried by AgNPs; the surface of AgNPs was positively charged.[40]

The FTIR spectra of organic functional groups on the surface of HA and AgNPs–HA are shown in Fig. 4(c), with different wave number assignments to the spectral bands.[41] HA alone offers a wider absorption band at 3133 cm^{-1}, mainly assigned to the stretching vibrations of O–H and N–H, while the absorption bands located at (1) 2828, (2) 2360, (3) 1603, (4) 1398, and (5) 1125 are ascribed to (1) the stretching vibrations of C–H structures in lipid carbon chains, (2) carboxylic acid–OH stretching vibrations, (3) stretching vibrations of conjugated C=C or H-bonded carbonyl C=O, (4) bending vibrations in the –OH plane of alcohols or phenols, and (5) stretching vibrations of C–OH; while the absorption bands located at 880 cm^{-1} and 773 cm^{-1} are mainly attributed to the bending vibrations of C=C in the benzene ring.[42] Comparing the FTIR spectrograms after the interaction with AgNPs, it can be seen that the composition of HA and AgNP–HA functional groups did not change significantly, they both contain hydroxyl, phenolic, and carboxyl groups and alcohol groups, but the difference is that –OH is located at 3133 cm^{-1}, and the C=C and C=O bands at 1603 cm^{-1} are drifted, and the conjoined –OH, amino and spectral peaks of the stretching vibration of –OH in carboxylic acid weakened, indicating that the main functional groups of HA-adsorbed AgNPs are hydroxyl, amino, and carboxyl groups, and the carboxyl group in HA and the hydroxyl group of the aliphatic group adsorbed on the surface of AgNPs and complexed with AgNPs, which is consistent with the results of Hao *et al.*[43]

3.4 Characterization and analysis of AgNP interaction with BSA and HA

As shown in Fig. 5(a), the wavelength scan of AgNPs interacting with BSA at a specific concentration and adding different concentrations of HA shows that a small amount of HA changes the reaction state between AgNPs and BSA. With the increase in HA concentration, the absorption peaks at the positions of AgNPs and BSA gradually disappear. The peaks at both places show an increasing trend to produce color enhancement. The addition of HA changed the presence of AgNPs and BSA in the solution: (i) there was competition between HA and BSA, and the addition of HA robbed the adsorption position of BSA on the surface of AgNPs, so the summit of BSA increased with the increase in HA concentration; (ii) a complex was formed between HA and BSA, and HA wrapped around the surface of BSA, masking the interaction of BSA with AgNPs in the solution, thus making the absorption summit of BSA gradually disappear.[44]

A comparison of Fig. 5(b) shows that the zeta potential of AgNPs at different pH values changes to a large extent after the addition of different concentrations of HA. At pH = 4.0, the zeta potential on the surface of AgNPs decreased to a certain extent after the simultaneous addition of BSA and HA compared to the AgNP–BSA solution without the addition of HA. The degree of zeta potential decrease was more significant with the increase in HA concentration, and the potential on the surface of AgNPs decreased from 18.3 mV to −4.2 mV when the HA concentration was 150 mg L^{-1}. The reason was that the excess addition of HA neutralized most of the positive charges on the surface of AgNPs; at this time, HA dominated in the solution, indicating that HA replaced the BSA molecules on the surface of AgNPs as a stabilizer wrapped around the surface of AgNPs.[44] It was found through experimental studies that with the gradual increase in solution pH, when pH = 6.0, the continued addition of HA in the AgNP–BSA solution increased the $|\zeta|$ of AgNPs with the increase in HA concentration, which stabilized the AgNPs in the solution. When the solution pH is alkaline, it can be seen by comparison that a small amount of HA addition could make the AgNPs in the solution more stable, and the stability of AgNPs does not fluctuate with the increase in HA concentration, indicating that the surface charge of AgNPs was little affected by the change in HA concentration.

The reason for the appearance of a significant difference in the surface charge and stability of AgNPs is the change in HA concentration in different solution environments. This is because in acidic environments, most of the BSA in solution is positively charged, and it adheres to the surface of AgNPs.[45] At

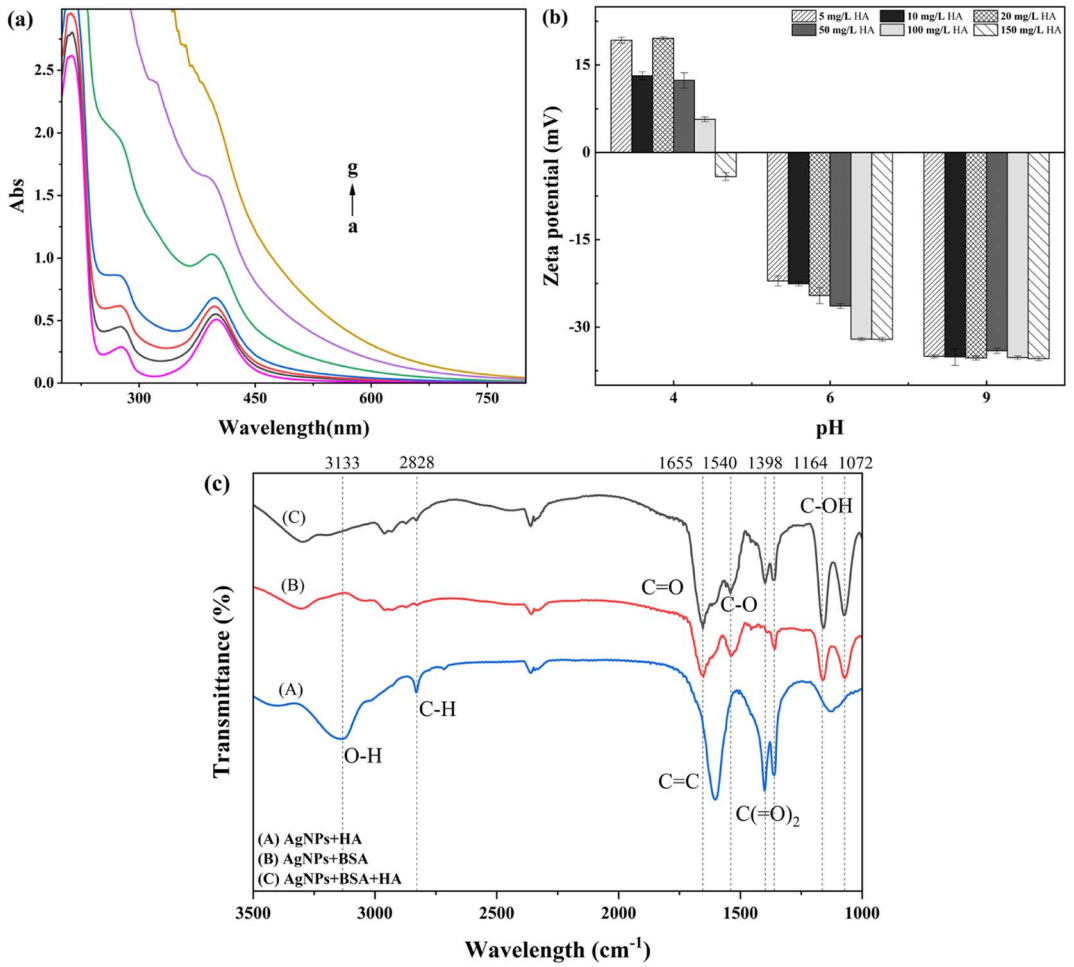

Fig. 5 (a) UV-vis spectra of AgNP–BSA complexes with different concentrations of HA. [AgNPs] = 3.774 mg L^{-1}, [BSA] = 300 mg L^{-1}, a–g: [HA] = 5, 10, 20, 50, 100, and 150 mg L^{-1}. (b) Effects of different concentrations of HA on the zeta potential of AgNP–BSA complexes. (c) Infrared spectra of AgNP–BSA before and after HA addition.

the same time, HA enters the solution with a large amount of negative charge, partly neutralized with BSA and partially adsorbed on the surface of AgNPs, thus changing the changeability of AgNPs to some extent and maintaining the system's stability. With the increase in solution pH, when the solution is neutral, at this time the solution pH is close to the solution pH of the prepared and obtained AgNPs, while HA can still be adsorbed on the modified nanoparticles *via* hydrophobic interactions, so the concentration of HA addition is positively correlated with the stability and surface charge of the AgNP amount.[36] The concentration of HA does not have a significant effect on the stability of AgNPs in an alkaline environment mainly because the prepared AgNP solution has excellent stability in an alkaline environment. A large amount of BSA will aggregate into macromolecules and reduce the stability of the system, but the addition of HA will limit the dissolution and aggregation of AgNPs by improving the charge on the particle surface in the solution,[36] thereby improving the stability of the system.[46]

The FTIR spectra of AgNPs with BSA or HA and AgNPs under the dual action of BSA and HA are shown in Fig. 5(c), where the concentration of BSA is 300 mg L^{-1}, and the concentration of HA is 100 mg L^{-1}. The comparison of the FTIR spectra of AgNPs under the dual action of BSA and HA and with the movement of BSA and HA alone shows that the absorption peak at 1398 cm^{-1}, while the absorption intensity of the C–O stretching vibration spectral peak at 1398 cm^{-1} decreases, and the spectral peak caused by the stretching vibration of O–H and N–H at 3133 cm^{-1} disappears, which proves that the joining-OH and C–O bonds are involved in the complex reaction between HA and BSA and dominate the response.[47] The comparison of the IR spectra of the interaction with AgNPs and BSA after the addition of HA revealed that the enhancement of the spectral peaks assigned to the C=O stretching vibration in the amide I band at 1655 cm^{-1} and the C–OH stretching vibration at 1164 cm^{-1} and 1072 cm^{-1} was due to the conjugation effect between C–OH, C=O, and HA, which increased the s component in the carbon atom hybridization orbitals. In comparison, it was found that the antisymmetric stretching of $C(=O)_2$ in the amide II band (COO^-) led to an increase in the vibrational frequency of the spectral peak of the carboxyl group at 1540 cm^{-1}. It is symmetric stretching at 1360 cm^{-1} and deepens the peak valley between

1255 and 1530 cm^{-1} due to the complexation of most carboxyl anion groups with nanoparticles through covalent bonds. Thus, the binding of BSA and AgNPs is tighter than that with HA.

4. Conclusions

This study used BSA and HA as simulants of dissolved organic matter in sewage treatment plants and used the concentration levels in sewage treatment processes as a reference to explore the changes in particle size and stability of AgNPs under the individual and combined effects of the two situations, the conclusion is as follows:

AgNPs can complex with the amino group, amide group, and carboxyl group in BSA to form AgNP–BSA complexes. With the gradual increase in BSA concentration, the particle size of AgNPs showed a trend of first decreasing and then increasing. When the concentration of BSA is 0–100 mg L^{-1}, the particle size of AgNPs in the system decreases. This is because the low concentration of BSA promotes the formation of Ag^{+} in the system to form AgNPs. When the BSA concentration continues to increase, the presence of BSA promotes the aggregation of AgNPs, resulting in an increase in the size of AgNPs in the system. The hydroxyl, amino, and carboxyl groups in HA can combine with AgNPs to form the AgNP–HA complex. As the HA concentration increases, the particle size and particle size distribution of AgNP particles increase. The hydrophobic group in HA enables it to better maintain the stability of silver nanoparticles in an acidic environment. When HA and BSA exist at the same time, HA will occupy the binding site between BSA and AgNPs or be wrapped on the surface of BSA, so that AgNP–HA dominates the system.

Exploring the interaction between AgNPs, proteins, and HA is an important basis for studying the migration and transformation of AgNPs in wastewater. In the future, more in-depth research is needed on the particle size, morphology, and complexation mechanism of AgNPs in order to prevent AgNPs from entering the aquatic environment and achieve ecological restoration.

Author contributions

Y. Q., J. K., and C. S.: investigation, methodology, formal analysis, data analysis, writing—original draft. Y. Q.: data analysis. C. S., and N. Z.: formatting & editing. Y. Q., and J. K.: methodology. P. Z., and N. Z.: prepare ESI Data. G. S.: conceptualization, resources, supervision, data curation, writing—review & final editing. All authors read and approved the final manuscript.

Conflicts of interest

There are no conflicts to declare.

Acknowledgements

The authors thank the Philosophy and Social Sciences Planning Project of Henan Province (No. 2018BTY021), Key Research Project Plan for Higher Education Institutions in Henan Province (No. 24B560011) for providing financial support necessary to carry out this work. The authors thank North China University of Water Resources and Electric Power for providing analytical instruments for this study.

References

1 E. McGillicuddy, I. Murray, S. Kavanagh, L. Morrison, A. Fogarty, M. Cormican, P. Dockery, M. Prendergast, N. Rowan and D. Morris, *Sci. Total Environ.*, 2017, **575**, 231–246.
2 N. B. Turan, H. S. Erkan, G. O. Engin and M. S. Bilgili, Nanoparticles in the aquatic environment: Usage, properties, transformation and toxicity—A review, *Process Saf. Environ. Prot.*, 2019, **130**, 238–249.
3 C. Forstner, T. G. Orton, P. Wang, P. M. Kopittke and P. G. Dennis, Wastewater Treatment Processing of Silver Nanoparticles Strongly Influences Their Effects on Soil Microbial Diversity, *Environ. Sci. Technol.*, 2020, **54**, 13538–13547.
4 R. Ding, L. Li, P. Yang, L. Luo, L. Li and Q. Wang, Assessing the environmental occurrence and risk of nano-silver in Hunan, China using probabilistic material flow modeling, *Sci. Total Environ.*, 2019, **658**, 1249–1255.
5 D. Shevlin, N. O'Brien and E. Cummins, Silver engineered nanoparticles in freshwater systems – Likely fate and behaviour through natural attenuation processes, *Sci. Total Environ.*, 2018, **621**, 1033–1046.
6 X. Li and J. J. Lenhart, Aggregation and dissolution of silver nanoparticles in natural surface water, *Environ. Sci. Technol.*, 2012, **46**, 5378–5386.
7 Y. Yin, X. Yang, X. Zhou, W. Wang, S. Yu, J. Liu and G. Jiang, Water chemistry controlled aggregation and photo-transformation of silver nanoparticles in environmental waters, *J. Environ. Sci.*, 2015, **34**, 116–125.
8 M. Millour, J.-P. Gagné, K. Doiron, I. Marcotte, A. A. Arnold and É. Pelletier, Effects of concentration and chemical composition of natural organic matter on the aggregative behavior of silver nanoparticles, *Colloids Surf., A*, 2021, 623.
9 S. Wang, Z. Liu, W. Wang and H. You, Fate and transformation of nanoparticles (NPs) in municipal wastewater treatment systems and effects of NPs on the biological treatment of wastewater: a review, *RSC Adv.*, 2017, **7**, 37065–37075.
10 G. Brunetti, E. Donner, G. Laera, R. Sekine, K. G. Scheckel, M. Khaksar, K. Vasilev, G. De Mastro and E. Lombi, Fate of zinc and silver engineered nanoparticles in sewerage networks, *Water Res.*, 2015, **77**, 72–84.
11 Z. Zhang, P. Gao, M. Li, J. Cheng, W. Liu and Y. Feng, Influence of Silver nanoparticles on nutrient removal and microbial communities in SBR process after long-term exposure, *Sci. Total Environ.*, 2016, **569–570**, 234–243.
12 N. Dasgupta, S. Ranjan, D. Patra, P. Srivastava, A. Kumar and C. Ramalingam, Bovine serum albumin interacts with silver nanoparticles with a "side-on" or "end on" conformation, *Chem.-Biol. Interact.*, 2016, **253**, 100–111.

13 D. J. Boehmler, Z. J. O'Dell, C. Chung and K. R. Riley, Bovine Serum Albumin Enhances Silver Nanoparticle Dissolution Kinetics in a Size- and Concentration-Dependent Manner, *Langmuir*, 2020, **36**, 1053–1061.
14 G. Qiu, K. Wirianto, Y. Sun and Y.-P. Ting, Effect of silver nanoparticles on system performance and microbial community dynamics in a sequencing batch reactor, *J. Cleaner Prod.*, 2016, **130**, 137–142.
15 B. Thalmann, A. Voegelin, E. Morgenroth and R. Kaegi, Effect of humic acid on the kinetics of silver nanoparticle sulfidation, *Environ. Sci.: Nano*, 2016, **3**, 203–212.
16 M. Bin Ahmad, J. J. Lim, K. Shameli, N. A. Ibrahim and M. Y. Tay, Synthesis of Silver Nanoparticles in Chitosan, Gelatin and Chitosan/Gelatin Bionanocomposites by a Chemical Reducing Agent and Their Characterization, *Molecules*, 2011, **16**, 7237–7248.
17 A. Sahraei, F. Mohammadi, R. Boukherroub and S. Szunerits, Formation of a Highly Stable and Nontoxic Protein Corona upon Interaction of Human α-1-Acid Glycoprotein (AGP) with Citrate-Stabilized Silver Nanoparticles, *Langmuir*, 2020, **36**, 10321–10330.
18 A. Rajeshwari, S. Pakrashi, S. Dalai, R. Madhumita, V. Iswarya, N. Chandrasekaran and A. Mukherjee, Spectroscopic studies on the interaction of bovine serum albumin with Al_2O_3 nanoparticles, *J. Lumin.*, 2014, **145**, 859–865.
19 N. Aihara, K. Torigoe and K. Esumi, Preparation and Characterization of Gold and Silver Nanoparticles in Layered Laponite Suspensions, *Langmuir*, 1998, **14**, 4945–4949.
20 S. R. D. P. Nandita Dasgupta, Bovine serum albumin interacts with silver nanoparticles with a "side-on" or "end on"Bovine serum albumin interacts with silver nanoparticles with a "side-on" or "end on"conformation, *Chem.-Biol. Interact.*, 2016, 100–111.
21 Z. S. Pillai and P. V. Kamat, What Factors Control the Size and Shape of Silver Nanoparticles in the Citrate Ion Reduction Method?, *J. Phys. Chem. B*, 2004, **108**, 945–951.
22 F. Polesel, J. Farkas, M. Kjos, P. Almeida Carvalho, X. Flores-Alsina, K. V. Gernaey, S. F. Hansen, B. G. Plósz and A. M. Booth, Occurrence, characterisation and fate of (nano)particulate Ti and Ag in two Norwegian wastewater treatment plants, *Water Res.*, 2018, **141**, 19–31.
23 Y. Dasaradhudu and M. Arunachalam Srinivasan, Synthesis and characterization of silver nano particles using co-precipitation method, *Mater. Today: Proc.*, 2020, **33**, 720–723.
24 Y. T. He, J. Wan and T. Tokunaga, Kinetic stability of hematite nanoparticles: the effect of particle sizes, *J. Nanopart. Res.*, 2008, **10**, 321–332.
25 E. Tombácz, G. Filipcsei, M. Szekeres and Z. Gingl, Particle aggregation in complex aquatic systems, *Colloids Surf., A*, 1999, **151**, 233–244.
26 A. M. Siddiq, D. Murugan, R. Srivastava and M. S. Alam, Influence of pH on interaction of silver nanoparticles – protein: Analyses by spectroscopic and thermodynamic ideology, *Colloids Surf., B*, 2019, **184**, 110524.
27 M. B. Espeche Turbay, V. Rey, R. D. Dorado, M. C. Sosa and C. D. Borsarelli, Silver nanoparticle-protein interactions and the role of lysozyme as an antagonistic antibacterial agent, *Colloids Surf., B*, 2021, **208**, 112030.
28 R. Binaymotlagh, H. Hadadzadeh, H. Farrokhpour, F. H. Haghighi, F. Abyar and S. Z. Mirahmadi-Zare, In situ generation of the gold nanoparticles–bovine serum albumin (AuNPs–BSA) bioconjugated system using pulsed-laser ablation (PLA), *Mater. Chem. Phys.*, 2016, **177**, 360–370.
29 Z. Zaheer, S. A. Kosa and M. Akram, Interactions of Ag+ ions and Ag-nanoparticles with protein. A comparative and multi spectroscopic investigation, *J. Mol. Liq.*, 2021, **335**, 116226.
30 S. H. Brewer, W. R. Glomm, M. C. Johnson, M. K. Knag and S. Franzen, Probing BSA Binding to Citrate-Coated Gold Nanoparticles and Surfaces, *Langmuir*, 2005, **21**, 9303–9307.
31 A. Gebregeorgis, C. Bhan, O. Wilson and D. Raghavan, Characterization of Silver/Bovine Serum Albumin (Ag/BSA) nanoparticles structure: Morphological, compositional, and interaction studies, *J. Colloid Interface Sci.*, 2013, **389**, 31–41.
32 A. Selva Sharma and M. Ilanchelian, Comprehensive Multispectroscopic Analysis on the Interaction and Corona Formation of Human Serum Albumin with Gold/Silver Alloy Nanoparticles, *J. Phys. Chem. B*, 2015, **119**, 9461–9476.
33 G. Wang, Y. Lu, H. Hou and Y. Liu, Probing the binding behavior and kinetics of silver nanoparticles with bovine serum albumin, *RSC Adv.*, 2017, **7**, 9393–9401.
34 X. Xu, X. Mao, Y. Wang, D. Li, Z. Du, W. Wu, L. Jiang, J. Yang and J. Li, Study on the interaction of graphene oxide-silver nanocomposites with bovine serum albumin and the formation of nanoparticle-protein corona, *Int. J. Biol. Macromol.*, 2018, **116**, 492–501.
35 A. R. Poda, A. J. Kennedy, M. F. Cuddy and A. J. Bednar, Investigations of UV photolysis of PVP-capped silver nanoparticles in the presence and absence of dissolved organic carbon, *J. Nanopart. Res.*, 2013, **15**(5), 1673–1679.
36 Y. Z. Ishara Fernando, Concentration dependent effect of humic acid on the transformations of silver nanoparticles, *J. Mol. Liq.*, 2019, 291–299.
37 N. Akaighe, S. W. Depner, S. Banerjee, V. K. Sharma and M. Sohn, The effects of monovalent and divalent cations on the stability of silver nanoparticles formed from direct reduction of silver ions by Suwannee River humic acid/natural organic matter, *Sci. Total Environ.*, 2012, **441**, 277–289.
38 Y. Wu and T. Cheng, Stability of nTiO 2 particles and their attachment to sand: Effects of humic acid at different pH, *Sci. Total Environ.*, 2016, **541**, 579–589.
39 J. Mariam, P. M. Dongre and D. C. Kothari, Study of Interaction of Silver Nanoparticles with Bovine Serum Albumin Using Fluorescence Spectroscopy, *J. Fluoresc.*, 2011, **21**, 2193–2199.
40 T. Zhao, M. Fang, Z. Tang, X. Zhao, F. Wu and J. P. Giesy, Adsorption, aggregation and sedimentation of titanium dioxide nanoparticles and nanotubes in the presence of different sources of humic acids, *Sci. Total Environ.*, 2019, **692**, 660–668.

41 L. Wang, Y. Lu, C. Yang, C. Chen, W. Huang and Z. Dang, Effects of Cd(II) on the stability of humic acid-coated nano-TiO2 particles in aquatic environments, *Environ. Sci. Pollut. Res.*, 2017, **24**, 23144–23152.

42 Y. Yao, N. Mi, C. He, H. He, Y. Zhang, Y. Zhang, L. Yin, J. Li, S. Yang, S. Li and L. Ni, Humic acid modified nano-ferrous sulfide enhances the removal efficiency of Cr(VI), *Sep. Purif. Technol.*, 2020, **240**, 116623.

43 Y. Hao, Z. Xu, J. Gao, K. Wu, J. Liu and J. Luo, Humic acid assisted chemical synthesis of silver nanoparticles for inkjet printing of flexible circuits, *J. Mater. Sci.: Mater. Electron.*, 2019, **30**, 20400–20409.

44 X. Wang, W. Fan, Z. Dong, D. Liang and T. Zhou, Interactions of natural organic matter on the surface of PVP-capped silver nanoparticle under different aqueous environment, *Water Res.*, 2018, **138**, 224–233.

45 T. Kopac, K. Bozgeyik and E. Flahaut, Adsorption and interactions of the bovine serum albumin-double walled carbon nanotube system, *J. Mol. Liq.*, 2018, **252**, 1–8.

46 X. Qi, Y. N. Dong, H. Wang, C. Wang and F. Li, Application of Turbiscan in the homoaggregation and heteroaggregation of copper nanoparticles, *Colloids Surf., A*, 2017, **535**, 96–104.

47 K. Quester, M. Avalos-Borja and E. Castro-Longoria, Controllable Biosynthesis of Small Silver Nanoparticles Using Fungal Extract, *J. Biomater. Nanobiotechnol.*, 2016, **07**, 118–125.